Electrical and Mechanical Properties of Bismuth Oxide Nanowire/Poly(vinyl acetate)

Waleed E. Mahmoud,* A. A. Al-Ghamdi

Department of Physics, Faculty of Science, King AbdulAziz University, Jeddah, Saudi Arabia

Received 14 September 2009; accepted 29 March 2010
DOI 10.1002/app.32523
Published online 3 June 2010 in Wiley InterScience (www.interscience.wiley.com).

ABSTRACT: Poly(vinyl acetate) (PVAc) loaded bismuth oxide (Bi_2O_3) nanowires was successfully prepared at low temperature and ambient pressure. X-ray diffraction and transmission electron microscopy were used to characterize the final product. It was found that Bi_2O_3 nanowires were formed and the diameter of the rods was confined to within 8 nm. The diameter and length of formed rods was found increase by increasing the bismuth oxide concentration in the PVAc matrix. The current-voltage (I-V) characteristic curves revealed that the charge transport is mainly nonlinear due to grain boundary contribution. The complex impedance spectroscopy was confirmed that the grain boundary effect controls the charge transport mechanism through nanocomposites. The deformation behavior after preparing the nanocomposites, irrespective of Bi_2O_3 concentration, is similar to that of the unfilled elastomer, implying that the mechanism of large deformation is mainly governed by the matrix. The mechanical measurements confirmed that the bismuth oxide has rod-like shape. © 2010 Wiley Periodicals, Inc. J Appl Polym Sci 118: 1598–1605, 2010

Key words: mechanical properties; nanocomposites; morphology

INTRODUCTION

Nanostructured materials constitute a rapidly growing field, in terms of both scientific interest and industrial application. Chemical structures and systems within the size range from 1 to 100 nm in one, two and three dimensions are typical for such materials. They are attracting considerable attention, because they present new challenges for the chemist. Nanoparticles may take on quite different shapes such as spheroids, mushrooms, platelets, rods or tubes, and the form adopted plays a large role in determining the basic properties,[1] for example, isotropic or anisotropic behavior and region-dependent surface reactivity.[2]

In recent years, an enormous amount of research work has been devoted to the study of one-dimensional (1D) nanostructure materials such as nanowires, nanotubes and nanobelts, due to their novel properties different from conventional bulk materials and potential applications in nanoscale electronic and optoelectronic devices.[3] Nanowires of various compositions have been synthesized using a wide variety of methods including carbothermal reactions, vapor–liquid–solid (VLS) growth, vapor–solid (VS) growth, template-assisted route, and solvothermal synthesis.[3] Moreover, some nanowires have been employed to construct such exciting systems as nanowire integrated systems[4] and nanolasers.[5] Considering the importance of metal oxides in catalysis, electrochemistry, optics, functional ceramics and sensors, their fabrication in 1D nanostructured morphology appears to be a particularly attractive goal.

Recently, bismuth oxide (Bi_2O_3) has been investigated extensively due to its optical and electrical properties such as refractive index, large energy band gap, dielectric permittivity as well as remarkable photoluminescence and photoconductivity. These properties make bismuth oxide an interesting candidate for applications in the fields such as optoelectronics, optical coatings, gas sensors, Schottky barrier solar cells, metal-insulator-semiconductor capacitors, microwave integrated circuits, etc. Bi_2O_3 shows four main structures that are denoted by α-, β-, γ-, and δ-Bi_2O_3.[6] The low-temperature α-phase and high-temperature δ-phase are stable, and the others are high-temperature metastable phases.[7] These special features explain the great effort devoted to the investigation of Bi_2O_3 polymorphs over the last years.

Typically Bi_2O_3 is prepared via the oxidation of bismuth metal at 800°C via thermal decomposition of carbonates or hydroxides produced by the addition of alkali-metal hydroxides to bismuth salt solution.[8–10] These powders on calcinations yield fine

**Present address:* Department of Physics, Faculty of Science, Suez Canal University, Ismailia, Egypt.
Correspondence to: W. E. Mahmoud (w_e_mahmoud@yahoo.com).

particles of Bi_2O_3. Flame spray pyrolysis[11] is also used to produce nano-sized Bi_2O_3 particles. The properties of ceramics are greatly affected by the characteristics of the powder, such as particle size, morphology, purity and chemical composition. Using chemical methods, e.g., coprecipitation, sol–gel, hydrothermal and colloid emulsion technique have been confirmed to efficiently control the morphology and chemical composition of prepared powders. Here, we report a simple urea-nitrate process for the preparation of nanowire Bi_2O_3. This method is commonly used for preparation of various oxides[12–15] and not yet reported for the preparation of Bi_2O_3 ceramics. Urea is used as a fuel, precipitating agent and as a resin former with formaldehyde. When urea is used along with nitrate salt of a cation and heated at 400°C, the exothermic reaction between nitrate (oxidant reactant) and urea (fuel) leads to formation of corresponding nanowire oxides.

To the best of our knowledge, no experimental work has been reported on the effect of Bi_2O_3 nanowire on polymeric materials. The future application of these materials strongly depends on the success of improving their mechanical and electrical properties. With this in mind, the purpose of the present contribution is to present new data for the effect of Bi_2O_3 nanowire on the electrical and mechanical properties of poly(vinyl acetate) (PVAc) as much detail as possible.

EXPERIMENTAL

Materials and processing

To synthesize Bi_2O_3 with the shapes of nanorods and nanowires, 0.3 mol bismuth nitrate pentahydrate ($Bi(NO_3)_3{\cdot}5H_2O$) was dissolved in 20 mL nitric acid and 0.5 mol urea (NH_2CONH_2) was dissolved in 30 mL de-ionized water. These two solutions were added to each other and kept refluxing on the magnetic stirrer at 120°C, until the mixture color changes to yellow; indicating the formation of bismuth oxide. The obtained powder was filtered and washed many times by de-ionizes water and left in an electric oven at 60°C to remove the solvent. Then the nanopwder calcined at 400°C.

A solution of poly(vinyl acetate) PVAc (average molecular weight 30,000 g mol^{-1}; obtained from Aldrich and used as received) was prepared by dissolving 6 g of PVAc into 100 mL benzene and kept stirring at 90°C for 3 h to give a viscous transparent solution. Required amount (0.1, 0.3, 0.5, 0.7, and 0.9%) of bismuth oxide was added to the polymer solution and kept stirring for 1 h at 90°C, after that they were cast in glass dishes and left to dry in a dry atmosphere at room temperature. Samples were transferred to an electric oven held at 60°C for 48 h to minimize the residual solvent. The thickness of the obtained films was in the range 0.2 mm.

Measurements

Transmission electron micrographs were obtained from Philips CM 12 transmission electron microscope (TEM). The colloidal solution containing Bi_2O_3 nanocrystals stabilized in the presence of PVAc was dropped over a carbon coated copper grid and dried in air at room temperature. The x-ray diffraction (XRD) pattern was measured using (A Philips PW 1370) x-ray diffractometer operating at 35 kV and 15 mA, using a monochromated Ni filter, radiation ($\lambda = 0.1789$ nm), a scanning rate of (2° min^{-1}), and a range of $20 < 2\Theta < 60$.

The stress–strain behavior in the case of uniaxial extension was measured at room temperature using a material tester (AMETEK) connected by a digital force gauge (Hunter Spring ACCU Force II, 0.01 *N* resolution) to measure the stress force. The force gauge was interfaced with a computer to record the obtained data. The stress–strain behavior was measured at a strain rate of 0.1 s^{-1}.

For electrical measurements the samples were made in the form of discs with 2 mm thick and 1 cm diameter. Silver paste was painted to the parallel faces of the samples as electrodes. In electrical measurements a digital electrometer (616 Keithly) was used. Aregulated noninductive furnace cell connected to a temperature controller (Digi-Sense, IL 60,010) was used to vary sample temperature from 30 to 180°C with constant rate of 2°C/min.

RESULTS AND DISCUSSION

TEM analysis

Figure 1 depicts a transmission electron microscopy (TEM) image of as-prepared PVAc loaded with 0.1, 0.5, and 0.9 wt % of Bi_2O_3. Bismuth oxide rods like shape were formed in the PVAc matrix with a diameter of 8.3 ± 0.6 nm, 19.4 ± 0.5 and 23.2 ± 1.4, respectively. On the other hand as the bismuth oxide content increases in the PVAc matrix, the rod length increases and mesh like shape had been formed. The average particle size for all nanocomposite films was presented in Table I.

For this work, the process of formation of Bi_2O_3 may be proposed as follows:

In acidic solution: Bi^{3+} + Urea → $[Bi(Urea)_3]^{3+}$ → Bi_2O_3 (yellow)

When $Bi(NO_3)_3{\cdot}5H_2O$ and urea were dissolved in nitric acid and de-ionized water, $[Bi(Urea)_3]^{3+}$ complexes formed. Subsequently, the $[Bi(Urea)_3]^{3+}$ complexes were decomposed at 120°C, and Bi_2O_3 yellow precipitates were produced.[16,17]

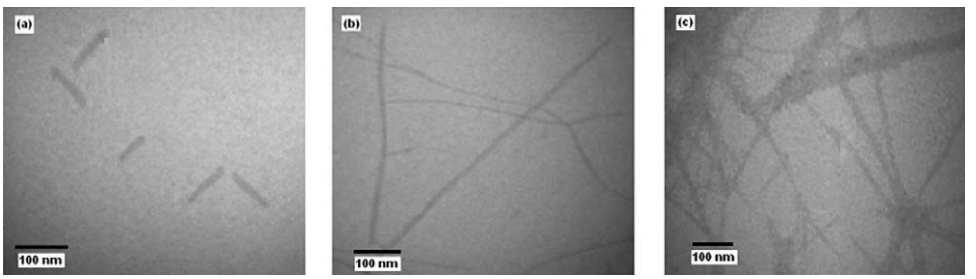

Figure 1 TEM image for bismuth oxide doped PVAc at different concentrations (a) 0.1 wt %, (b) 0.5 wt % and (c) 0.9 wt %.

The acidities have a strong influence on the product morphologies, controlled by the nucleation and growth processes. In acid-free solution, the product was irregular shape (result not shown). It is in accordance with those synthesized by Lu et al.[18] and Dong et al.,[19] and the precipitates were expected to be $BiONO_3$.[19] When 20 mL of HNO_3 was added to the solution the reaction rate became much faster, and a number of Bi_2O_3 nuclei formed. The nuclei were so many that they clustered into spherical cores[16] with active sites on the surfaces. As time passed, Bi_2O_3 nanorods grew out of the active sites on the spheres, and nanorods were finally produced, due to their inherent chain-type structure.

XRD analysis

XRD pattern of poly(vinyl acetate) doped bismuth oxide at concentrations ranging from 0.1 to 0.9 wt % is shown in Figure 2 for 2Θ values of 20 to 60°. This figure shows that the bismuth oxide diffraction peaks decreases in intensity due to the embedded into poly(vinyl acetate) with an incremental broadening of the peaks. This can be attributed to the reduction in intermolecular interaction between PVAc chains on incorporating Bi_2O_3. Above a minimum fraction of Bi_2O_3 content (from 0.7 wt % upwards), the samples exhibit additional peaks apart from those below 0.7 wt %. Sample 0.9 wt %, maximum Bi_2O_3 content, exhibits Bi_2O_3 reflection peak shaper than other samples. On indexing the peaks the samples showed the pattern and the observed d lines match the reported values for the β-Bi_2O_3 phase (JCPDS no. 27–50). The calculated lattice parameters by least square fit are $a = 7.732$ Å and $c = 5.618$ Å. The average particle size for nanocomposite films was calculated by using Scherrer formula[20]

$$d = \frac{k\lambda}{\beta \cos\theta} \quad (1)$$

where k is a constant which is taken to be 0.9, λ the wavelength of x-rays used (0.1789 nm), β the full width at half maximum (FWHM) and Θ is the angle of diffraction. The average diameter of nanocomposite films was presented in Table I. From such table, it is clear that the average particle sizes matche well those obtained from TEM.

TABLE I
The Particle Size of Bi_2O_3 Nanoparticles Embedded Into PVAc Matrix

Bi_2O_3 concentration (wt %)	TEM Particle size (nm)	XRD Particle size (nm)
0.1	8.30 ± 0.60	8.23
0.3	12.10 ± 0.20	12.20
0.5	19.40 ± 0.50	19.50
0.7	21.10 ± 0.20	21.20
0.9	23.20 ± 1.40	23.80

Electrical properties

The percolation threshold is a basic characteristic of a conductive composite; in this case the percolation threshold defines the composition range for studying the effect of Bi_2O_3 on conductivity. Figure 3 shows the

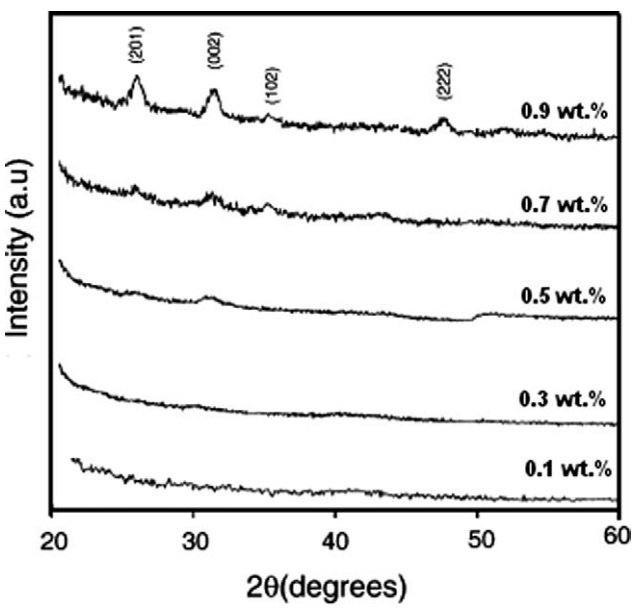

Figure 2 XRD for PVAc loaded different concentrations of bismuth oxide.

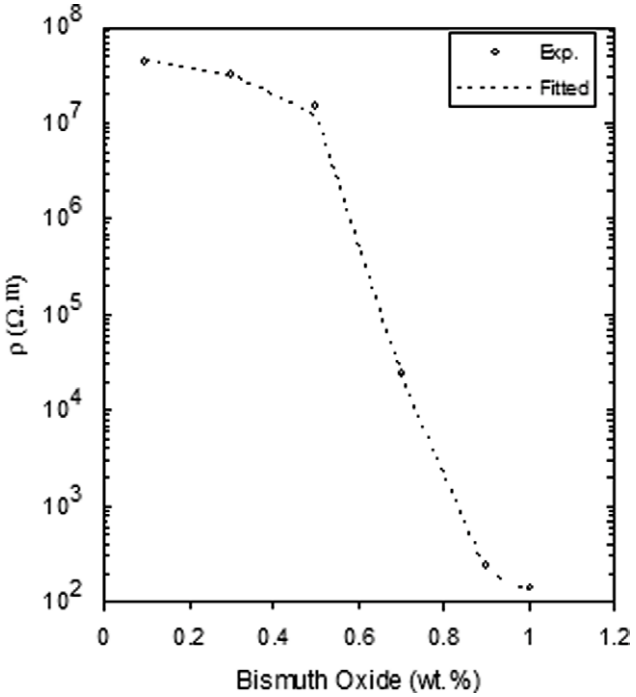

Figure 3 The resistivity vs. bismuth oxide content.

variation of the resistivity with the volume fraction of filler. A typical S-shaped curve is observed that separates three regions: insulating, transition, and conductive. The model that is most often used to quantify the changes in the transition and conductive regions is the so-called statistical percolation model.[21] Proposed by Kirkpatrick[22] and Zallen,[23] this model predicts the electrical resistivity of an insulator-conductor binary mixture by assuming random positions of the filler particles. The result is a power-law variation of the resistivity ρ, above the percolation threshold:

$$\rho\alpha\left(\frac{V - V_C}{1 - V_C}\right)^{-t} \tag{2}$$

where V is the volume fraction of filler, V_c the percolation threshold and t is a universal exponent that is close to 2 for a 3D dispersion.[24] The two parameters fit are represented in Figure 3 by the dotted line and gives $V_c = 0.7$ and $t = 2.01$. The value of the exponent t is consistent with the model prediction. The significant point here is that the percolation concentration is low comparing with nano-spherical particles. It may be attributed to the tendency of nano-spherical particles to aggregates in the polymer matrix, while nanorods have low tendency to aggregates and dispersed well into the polymer matrix.

The I–V characteristics of the PVAc loaded different concentrations of biamuth oxide nanowire are shown in Figure 4. The I–V behavior is linear (i.e., ohmic) at small voltages and becomes nonlinear above a certain voltage, which is typical of a varistor-like device. The α values were obtained from the I–V curve in the nonlinear region, by a linear fit for the log I versus log V data according to the relation $I = KV^{\alpha}$. The values of nonlinear coefficient α are given in Table II. These data show that the values of α decreased as the bismuth oxide concentration increase. Since, the grains are much larger in size and the grain surface area is much smaller. This enhancement of density and intergrain contacts leads to lower resistivity in the nanocomposite. Therefore, one can conclude that there is a strong correlation between the ceramic grain structure and the values of resistivity and α. The α value of the ceramic is higher when the resistivity is higher (when Bi_2O_3 concentration is low in PVAc matrix), which is attributed to smaller grain size and hence larger grain surface area. When Bi_2O_3 concentration increase, the resistivity will decreased and the α value will become much smaller (compared to low concentrations). The highly nonlinear I–V characteristics indicate a tunneling type transport mechanism across a highly resistive potential barrier created by the grain boundary and the intergrain distance.[25]

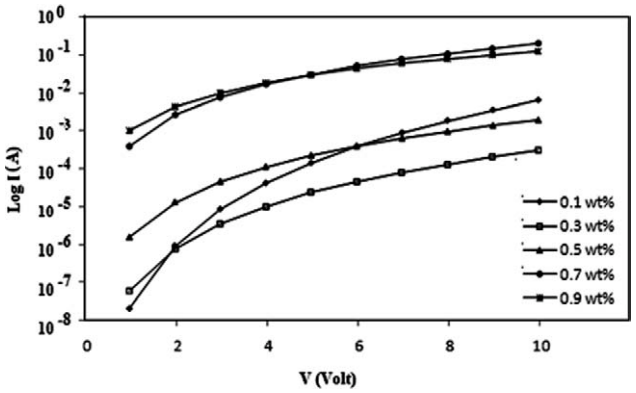

Figure 4 The I-V characteristic curves of nanocomposites.

Let us now consider the complex impedance spectroscopy which is a powerful tool in separating out the bulk and grain boundary effects. The impedance spectra of nanocomposites is measured and presented in Figure 5(a). This figure indicates that, the spectrum exhibits two semicircles. The low frequency semicircle was interpreted as due to the grain boundary effects

TABLE II
The Calculated Values of Nonlinear Coefficient (α), Grain Resistance (R_g) and Grain Boundary Resistance (R_{gb}) of Bi_2O_3/PVAc Nanocomposite Films

Bi_2O_3 concentration (wt %)	α	R_g Ω	R_{gb} Ω	R_{gb}/R_g
0.1	5.50	30	3.2×10^8	1.06×107
0.3	3.68	40	1.4×10^6	3.50×104
0.5	3.09	50	1.3×10^4	260
0.7	2.70	72	2.6×10^2	3.60
0.9	2.11	80	150	1.87

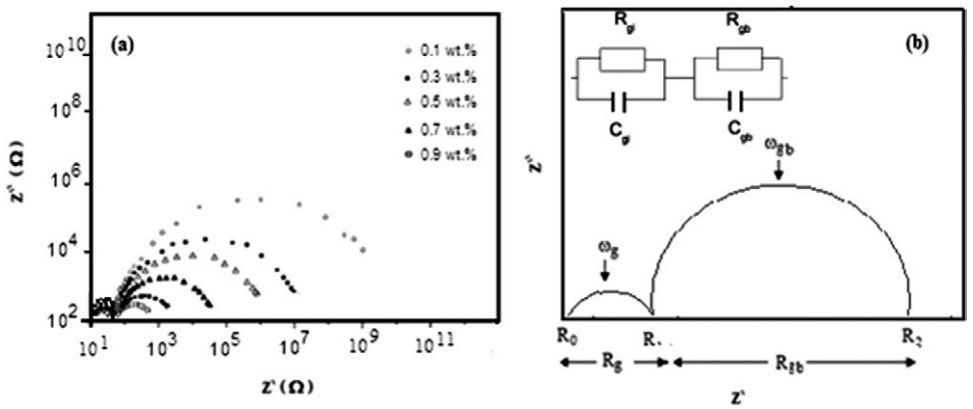

Figure 5 Impedance spectra of nanocomposites.

and the higher frequency semicircle due to the nano grain interior.[26] According to Maxwell-Wagner two-layer equivalent circuit model,[27] the high frequency semicircle was due to the contribution from the grain boundaries. The modified Cole–Cole expression,[28] for the distribution of impedance based on the two-layer model, in which the complex impedance $Z^*(\omega)$ consists of two coincide semicircles, can be written as

$$Z^*(\omega) = R_o + \frac{R_1 - R_o}{1 + (i\omega\tau_g)^{1-\alpha_g}} + \frac{R_2 - R_1}{1 + (i\omega\tau_{gb})^{1-\alpha_{gb}}} \quad (3)$$

where R_o, R_1 and R_2 are the intercepts with the real impedance axis of the high frequency and low frequency semicircle ends as indicated in Figure 5(b). τ_g and τ_{gb} are the mean relaxation times for the grain and grain boundary conduction processes, respectively. α_g and α_{gb} are two parameters indicate the deviation of the impedance plot shape from the ideal semicircular shape of the Debye model for the grain and grain boundary, respectively.

The values of R_g and R_{gb} represent the contributions to the total resistance of the sample by the grains and grain boundaries, which are given by the diameters of the semicircles. The ratio of R_{gb}/R_g can directly show the difference of grain and grain boundary resistance. As can be seen from Table II, the samples with higher ratio of R_{gb}/R_g exhibit electrical properties and the samples with lower ratio of R_{gb}/R_g exhibit approximately linear electrical properties. This is attributed to the trapping of electrons by the localized states within or at the grain boundaries of nanocrystalline Bi_2O_3. Grain boundaries in nanostructured metal oxides contain a large number of interface states localized between two adjacent grains. Such interface states are possibly created by dislocations introduced by crystallographic mismatch between the adjacent grains, thereby leading to dangling bonds or other interfacial defects.[29,30] All the traps present in grain boundaries capture free electrons from the adjoining grains.[31,32] For nano-Bi_2O_3 of small grain sizes which are less than the Debye length (22 nm for nano-Bi_2O_3[9]), bulk grains can be fully depleted by the traps and the whole specimen may behave like a compensated semiconductor with nonuniform spatial trap distribution. This results in the accumulation of electrons at the grain boundary region, which become electrically active, causing the enhanced conductivity of the grain boundary region. In this contribution, since the grain size of nano-Bi_2O_3 (at low concentrations) is less than the Debye length, the trap-limited process might be more predominant. The conduction along the grain boundaries is attributable to the trapping and detrapping,[33] and nearest-neighbor hopping of electrons.[34]

Figure 6 shows the variation of electrical conductivity with temperature for PVAc loaded different concentrations of bismuth oxide. Several features are

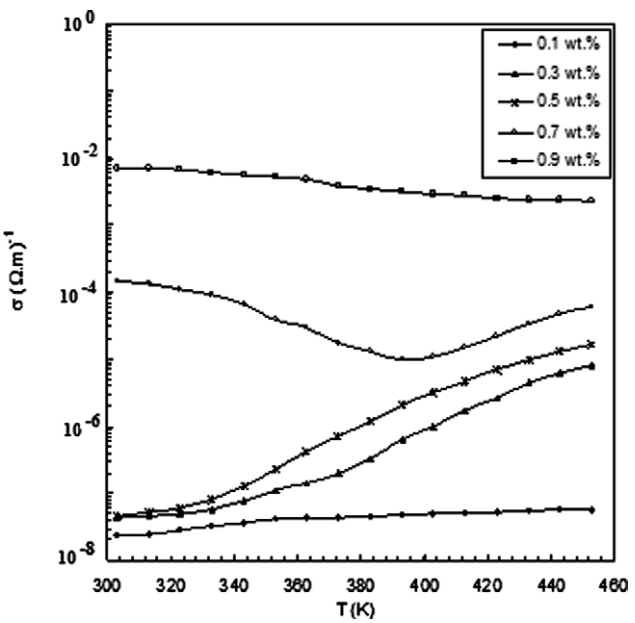

Figure 6 The variation of electrical conductivity with temperature for PVAc loaded different concentrations of bismuth oxide.

TABLE III
The Calculated Values of NTCC, PTCC, I_{NTCC}, and I_{PTCC} of Bi_2O_3 /PVAc Nanocomposite Films

Bi_2O_3 concentration (wt %)	NTCC (10^{-3} °C^{-1})	PTCC (10^{-3} °C^{-1})	I_{NTCC}	I_{PTCC}
0.1	–	0.02	–	0.39
0.3	–	1.12	–	2.28
0.5	–	1.64	–	2.42
0.7	7.12	3.01	1.16	2.77
0.9	4.49	–	0.50	–

observed, the first, all samples below the percolation concentration (from 0.1 to 0.5 wt %) exhibits PTCC (i.e., positive temperature coefficient of conductivity), this means that the conductivity increases against temperature. The second, the samples above percolation concentration (0.9 wt %) exhibits i.e., negative temperature coefficient of conductivity (NTCC), this means that the conductivity decreases against temperature. The third, sample 0.7 wt %, which belongs to the region of percolation concentration, exhibits NTCC up to temperature 393 K and after this temperature it exhibits PTCC.

From such behavior one can conclude that, at low concentrations the distance between bismuth oxide nanorods is large, results in an increase of the electrons hopping path, as the temperature increase there will be a completion between thermal activation and polymer expansion, until certain temperature 340 K the thermal activation is the predominant results in an increase of the conductivity. At high concentration the distance between bismuth oxide nanorods is very small and the distribution of bismuth oxide becomes in the form of mesh like shape as shown in TEM figure. As the temperature increase the polymer expanded results in a destruction of this mesh, so the hopping path of electrons decrease and the conductivity decrease in turn.

At percolation concentration the sample has both behavior, a decrease in the conductivity due to the polymer expansion up to 393 K and then increase in conductivity as a result of thermal activation.

The NTCC and PTCC can be estimated according to the equation:

$$(\mathrm{NTCC}, \mathrm{PTCC}) = \pm\left(\frac{1}{\sigma}\right)\left(\frac{d\sigma}{dT}\right) \tag{4}$$

NTCC and PTCC values for all samples are recorded in Table III.

To compare the NTCC and PTCC intensity quantitatively, the NTCC intensity (I_{NTCC}) and the PTCC intensity (I_{PTCC}) is defined as[35]:

$$I_{\mathrm{NTCC}} = \log\left(\frac{\sigma}{\sigma_{RT}}\right) \tag{5}$$

where σ and σ_{RT} are the conductivities at higher and at room temperature respectively. The NTCC and PTCC intensities were calculated and summarized in Table III.

It is found that PTCC increase with increasing bismuth oxide concentrations while NTCC decrease with increasing bismuth oxide concentrations. This indicates that bismuth oxide increases the ordering and/or texturing of the polymer matrix as mentioned earlier. This means that PVAc/Bi_2O_3 nanocomposites can be used as NTCC and PTCC thermistors.

Mechanical properties

Stress–strain behavior

Figure 7 shows the stress–strain curves obtained with various amounts of bismuth oxide dispersed in the PVAc matrix. The stress–strain curves were fitted by the Ogden model[36] and plotted in Figure 7.

$$\sigma = \frac{2\mu_1}{\alpha_1}\left([1+\varepsilon]^{\alpha_1-1} + [1+\varepsilon]^{-\left(\frac{\alpha_1}{2}+1\right)}\right) \tag{6}$$

where $\mu_1 = \mu_o = E_o/2(1+\nu) = E_o/3$ for an incompressible material, with E_o and ν being Young's modulus at the small strain deformation state and Poisson's ratio, respectively. σ is the applied stress and ε is the strain. α_1 is a material parameter depends on the host polymer.

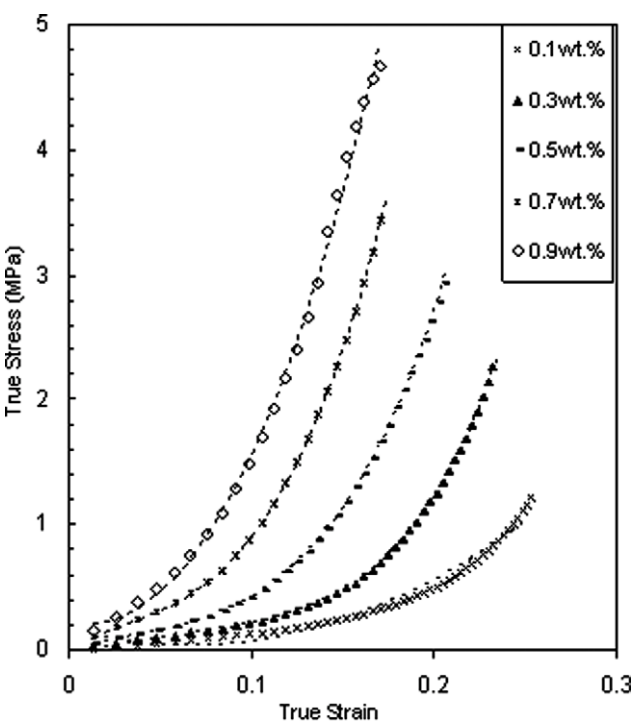

Figure 7 The stress–strain curves for all polymer samples; --- line represents the fitted curves by the Ogden model.

TABLE IV
The Fitted Parameters of the Ogden Model for Stress–Strain Behavior

Sample	0.1 (wt %)	0.3 (wt %)	0.5 (wt %)	0.7 (wt %)	0.9 (wt %)
μ_1 (MPa)	0.30 ± 0.02	0.83 ± 0.03	1.65 ± 0.12	2.69 ± 0.13	4.16 ± 0.13
α_1	1.2 ± 0.03	1.2 ± 0.04	1.2 ± 0.08	1.2 ± 0.07	1.2 ± 0.03

The fitting parameters, which are derived from the Ogden model, for all samples are presented in Table IV. From such table, it was found that by increasing the concentration of filler, a gradual improvement in modulus was observed. The results were compared with the Guth reinforcement model.[37] The model for spherical reinforcing particles has the form:

$$E = E_o(1 + 2.5V + 14.1V^2) \quad (7)$$

An alternative formulation accounts for nonspherical particles. For rod-like particles of aspect ratio f, the reinforcement is given by[38]:

$$E = E_o(1 + 0.67fV + 1.62f^2V^2) \quad (8)$$

Using f as an adjustable parameter, an excellent fit was obtained with $f = 7$, Figure 8. The importance of particle–particle interactions was inferred from the need for the second term in eq. (8), to describe the mechanical reinforcement. These results confirm the TEM photographs for rod-like shape.

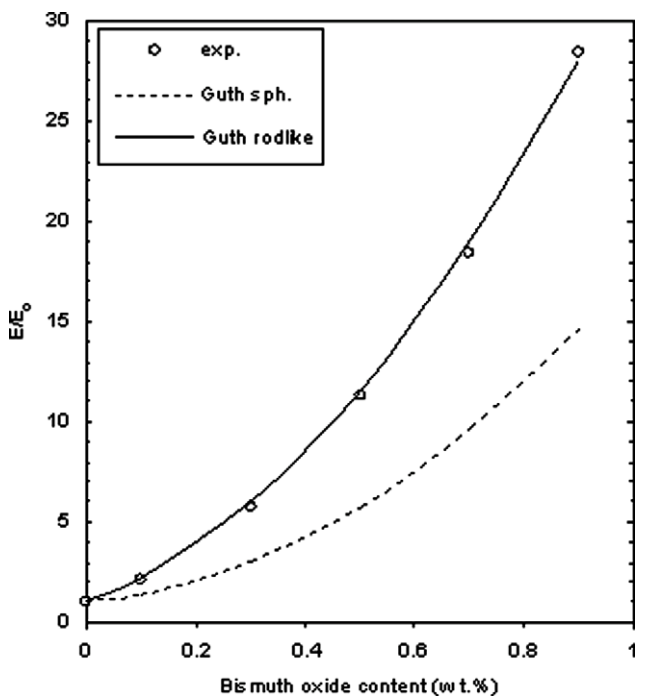

Figure 8 The relative modulus (E/E_o) as a function of bismuth oxide volume fraction.

Effect of tensile strain on electrical conductivity

Figure 9 represents the relative conductivity (σ/σ_o), as a function of tensile strain for all nanocomposites. From such a figure, it is found that σ/σ_o increases linearly with the applied load in certain range; after it the change is marginal. The change of σ/σ_o results in the change in hopping distance between Bi_2O_3 nanowires during the applied strain. This distance is determined according to eq. (9) and presented in Table V.

$$\varphi^{\frac{1}{3}} = \frac{D \times (L - D)}{(D + a) \times L} \quad (9)$$

where L is the sample length, D the particle size of the conducting filler and a is the interdomain distance which depends on the concentration of conducting phase (φ).[39,40]

Table V indicates that during application of tensile strain the interparticle distance changes giving rise

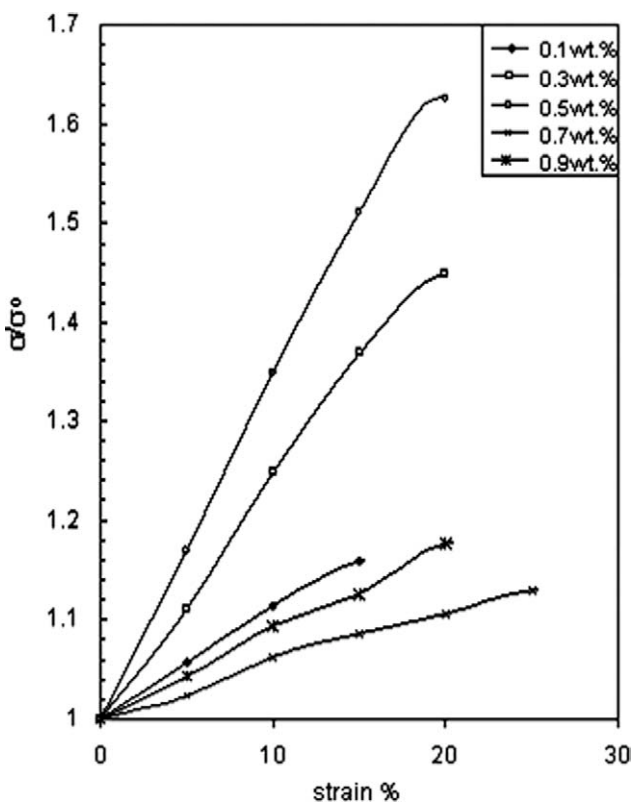

Figure 9 The relative conductivity (σ/σ_o) as a function of tensile strain for nanocomposite films.

TABLE V
The Interparticle Distance Between Bi_2O_3 Nanowires for All Nanocomposites Under the Effect of Tensile Strain

Bi_2O_3 concentration (wt %)	a (nm)			
	Strain = 5%	Strain = 10%	Strain = 15%	Strain = 20%
0.1	125 ± 2	130 ± 1	134 ± 2	137 ± 2
0.3	119 ± 3	121 ± 2	128 ± 2	130 ± 3
0.5	99 ± 1	102 ± 3	112 ± 4	121 ± 6
0.7	81 ± 5	126 ± 5	145 ± 4	163 ± 3
0.9	76 ± 3	89 ± 4	106 ± 1	117 ± 2

to a rapid change in electrical conductivity. Thus, a small change in (*a*) gives rises to a large change in (σ). To get maximum piezo-sensitivity, the value of (*a*) should be optimum since its change with applied strain will decide the change in sample resistance.[41] For low concentrations of Bi_2O_3, (*a*) will be large and change in (*a*) small while at high concentrations, (*a*) is small and change in (*a*) is large. Accordingly, the piezo-sensitivity will also change according to composition and it shows the maximum value at a certain critical composition, 0.7 wt %, at which (*a*) is optimized.

CONCLUSION

Different concentrations of nanoscale Bismuth oxide doped poly(vinyl acetate) was successfully prepared. The nanocomposites were characterized by TEM and XRD. The results have been indicated that β-Bi_2O_3 phase in the form of rod-like shape. The diameter and length of bismuth oxide was increased as its concentration in the PVAc matrix increase. The typical I-V characteristic curve of the nanocomposites is indicated a nonohmic behavior. This nonlinearity is due to the grain boundary effect. The complex impedance spectroscopy confirmed that the charge transport mechanism is mainly governed by grain boundary effect. The percolation concentration was found equal to 0.7 wt %. All samples below this concentration have PTCC, above it have NTCC and at the percolation has both behaviors. These results indicate that PVAc loaded bismuth oxide can be used as a thermistor. The mechanical measurements confirmed that the bismuth oxide in the form as rod-like shape which agrees with the TEM results. The polymer contains 0.7 wt % of bismuth oxide nanowire was the most sensitive to tensile strain variation.

References

1. Duan, X.; Huang, Y.; Agarwal, R.; Lieber, C. M. Nature 2003, 421, 241.
2. Mahmoud, W. E.; Hafez, M.; El-Aal, N. A.; El-Tantawy, F. Polym Int 2008, 7, 35.
3. Rao, C. N. R.; Deepak, F. L.; Gundiah, G.; Govindaraj, A. Prog Solid State Chem 2003, 31, 5.
4. Huang, Y.; Duan, X.; Cui, Y.; Lauhon, L.; Kim, K.; Lieber, C. M. Science 2001, 294, 1313.
5. Huang, M.; Mao, S.; Feick, H.; Yan, H.; Wu, Y.; Kind, H.; Weber, E.; Russo, R.; Yang, P. Science 2001, 292, 1897.
6. Khanna, P. K.; Singh, N.; Charan, S.; Viswanath, A. K.; Patil, K. R. Mater Res Bull 2007, 42, 1414.
7. Pendyala, N. B.; Koteswara Rao, K. S. R. J Lumin 2008, 128, 826.
8. Moens, L.; Ruiz, P.; Delmon, B.; Devillers, M. Catal Lett 1997, 46, 93.
9. Keuger, J.; Winkler, P.; Luderitz, E.; Luck, M.; Wolf, H. U. Ullmann's Encyclopedia of Industrial Chemistry; Wiley-VCH: Verlag GmbH, Weinheim, Germany, 2000.
10. Liu, A. T.; Kleinschmidt, P. Novel Ceramic Fabrication Process and Applications, Davidge, R. W., Ed. Institute of Ceramics: Staffs, UK, 1986; Vol. 38, pp 1–10.
11. Madler, L.; Pratsinis, S. E. J Am Ceram Soc 2002, 85, 1713.
12. Zanetti, S. M.; Santiago, E. I.; Bulhoes, L. O. S.; Varela, J. A.; Leite, E. R.; Longo, E. Mater Lett 2003, 57, 2812.
13. Yu, X.; Zhou, C.; He, X.; Peng, Z.; Yang, S. P. Mater Lett 2004, 58, 1087.
14. Ko, T.; Hwang, D. K. Mater Lett 2003, 57, 2472.
15. Ibrahim, D. M.; Mostafa, A. A.; Khalil, T. Ceram Int 1999, 25, 697.
16. Lu, J.; Han, Q.; Yang, X.; Lu, L.; Wang, X. Mater Lett 2007, 61, 2883.
17. He, R.; Qian, X.; Yin, J.; Zhu, Z. J Cryst Growth 2003, 252, 505.
18. Lu, J.; Han, Q.; Yang, X.; Lu, L.; Wang, X. Mater Lett 2007, 61, 3425.
19. Dong, L.; Chu, Y.; Zhang, W. Mater Lett 2008, 62, 4269.
20. Mahmoud, W. E.; El-Mallah, H. M. J Phys D: Appl Phys 2009, 4, 035502.
21. Lux, F. J Mater Sci 1993, 28, 285.
22. Kirkpatrick, S. Rev Mod Phys 1973, 45, 574.
23. Zallen, R. The Physics of Amorphous Solids; Wiley: New York, 1985.
24. Derrida, B.; Stauffer, D.; Herrmann, H. J.; Vannemius, J. J Phys Lett 1983, 44, 701.
25. Gross, R.; Alff, L.; Büchner, B.; Freitag, B. H.; Höfener, C.; Klein, J.; Lu, Y.; Mader, W.; Philipp, J. B.; Rao, M. S. R.; Reutler, P. Mater Lett 2002, 57, 887.
26. Greuter, F.; Blatter, G. Semi-Cond Sci Technol 1990, 5, 111.
27. Olsson, E.; Falk, L. K.; Dunlop, G. L.; Osterlund, R. J Mater Sci 1985, 20, 4091.
28. Pike, G. E. Mater Res Soc Symp Proc 1982, 5, 369.
29. Gupta, T. P. J Am Ceram Soc 1990, 73, 1817.
30. Einzinger, R. Annu Rev Mater Sci 1987, 17, 299.
31. Morris, W. G. J Vac Sci Technol 1976, 13, 926.
32. Bernasconi, J.; Strassler, S.; Knecht, B.; Klein, H. P.; Menth, A. Solid State Com 1977, 21, 867.
33. Mahan, G. D.; Levinson, L. M.; Philipp, H. R. J Appl Phys 1979, 50, 2799.
34. Mahmoud Waleed, E.; El-Eraki, M. H. I.; El- Lawindy, A. M. Y.; Hassan, H. H. J Phys D: Appl Phys 2006, 39, 2427.
35. Blythe, A. R. Electrical Properties of Polymers; Cambridge University Press: Cambridge, 1980; p 51.
36. Sau, K. P.; Chaki, T. K.; Khastgir, D. Pol Comp 1998, 29, 363.
37. Guth, E. J Appl Phys 1945, 16, 20.
38. Luginsland, H. D. Kautsch Gummi Kunstst 2000, 53, 10.
39. Hasse, A.; Klockmann, O.; Wehmeier, A. Kautsch Gummi Kunstst 2002, 55, 236.
40. Reuvekamp, L. A. E. M.; Ten Brinke, J. W.; Van Swaaij, P. J. Kautsch Gummi Kunstst 2002, 55, 41.
41. El-Lawindy, A. M. Y.; Abdel-Kader, K. M.; Mahmoud, W. E.; Hassan, H. H. Polym Int 2002, 51, 601.